https://doi.org/10.2352/EI.2026.38.6.ISS-285

Asynchronous Event-Based Sensors: A Case Study for Infrared Readout Integrated Circuits

Roman Fragasse, Megan Manifold, Ramy Tantawy, Shane Smith, Jonathan Bergey; SenseICs Corporation, Columbus, Ohio, USA

Abstract

Event-driven imaging enables low-latency, high-throughput sensing by reporting only temporal changes in a scene. A comparison of event-based and frame-based cameras under I/O-limited conditions shows that event-driven sensors achieve higher effective frame rates and lower latency in sparse scenes, while approaching frame-based limits as scene activity increases. Extending event-driven sensing to infrared (IR) wavelengths is challenged by elevated dark current and background-induced photocurrent. The limitations of conventional logarithmic (LOG) front-ends are analyzed, and performance is compared with a linear (LIN) front-end exhibiting stable conversion gain under high background conditions. Results indicate improved contrast sensitivity and minimum event temperature at high background, with LOG and LIN architectures each providing advantages over different background regimes.

Introduction

Event-driven cameras are bio-inspired sensors that represent a new paradigm in imaging. Unlike conventional cameras, which sample the scene at fixed integration intervals, event-driven sensors produce output only when a sufficient change in the scene is detected. As a result, the camera output is no longer a synchronous stream of "frames" representing approximate pixel intensities, but instead an asynchronous stream of "events" that encode temporal changes in each pixel. While event-driven cameras remain an active area of research, much of the foundational work has been conducted in the visible spectral range, originating from Prof. Carver Mead's research group at Caltech [1, 2, 3]. Building on this early work, several established imaging companies have further advanced the technology, producing megapixel-scale ($>$ 1 MP) sensors that integrate both frame-based and event-driven modalities on a single chip [4].

Despite advances in CMOS technology that have improved pixel pitch, power, throughput, and array format, the core event-driven pixel architecture remains largely unchanged from the original approach introduced by Prof. Mead [3]. Both early and modern designs employ a logarithmic transimpedance amplifier (TIA) front-end for high gain and wide dynamic range, often exceeding 120 dB [2, 3, 5], coupled with a self-resetting change detector (CD) back-end for in-pixel thresholding and event generation. The resulting events are processed peripherally and encoded using an address-event representation (AER) for transmission to downstream systems [6, 7].

Event-driven cameras capture only temporal changes in a scene, offering significant advantages when replacing or augmenting conventional frame-based imagers [4]. In frame-based systems, achieving low-latency at a fixed resolution typically requires increasing the frame rate, which in turn increases data throughput and power consumption. In contrast, event-driven sensors decouple latency from global readout rate; latency is instead governed by pixel-level response time and the instantaneous number of pixels undergoing a change in intensity. As a result, event cameras can capture fast temporal activity at substantially lower effective data rates. This efficiency arises from the inherent sparsity of natural scenes, where only a subset of pixels exhibit significant change at any given time. By transmitting only these changes, event-driven sensors reduce redundant data and enable low-latency operation without the high bandwidth requirements of frame-based approaches. This capability supports new modes of operation and enables a broad range of emerging applications [8].

Event-based imaging is also of significant interest in the infrared (IR) spectrum and has received substantial programmatic support in the United States [9]. This emphasis reflects the need to extend event-driven sensing to longer wavelengths, particularly in the MWIR and LWIR bands, where current solutions remain limited. However, scaling event-based architectures to these spectral regimes is challenging due to dark current and background-induced photocurrent, which are orders of magnitude higher than in visible-band sensors [10].

The success of event-driven cameras in the visible spectrum is largely enabled by the now-established logarithmic pixel front-end. This architecture provides very high transimpedance gain ($>$ 170 dBΩ) under low photocurrent conditions. However, due to its compressive logarithmic response, the effective gain decreases as the total input current increases. This behavior complicates direct application of the conventional front-end in IR regimes, where both background-induced photocurrent and thermally generated dark current increase substantially with wavelength and operating temperature.

In contrast to the conventional logarithmic front-end, a linear front-end can be used to maintain stable transimpedance gain as background-induced photocurrent and dark current increase. This capability enables high conversion gain in infrared sensors, which is essential for achieving sensitivity levels comparable to established visible event-driven sensors. A key performance metric for event-based sensors is contrast sensitivity (CS), defined as the ability to resolve small signal variations relative to the combined background and dark current. By preserving high conversion gain under elevated background conditions, linear front-end pixels improve contrast sensitivity and enable the detection of small temperature variations in emissive infrared scenes. This work, to the authors' knowledge, is the first to analyze the suitability of a baseline logarithmic architecture (LOG) versus a linear front-end architecture (LIN) for event-driven IR sensing under high dark current and background photocurrent conditions, with the goal of achieving optimal event sensitivity.

Frames vs. Events in I/O Limited Cameras

Over the past several decades, extensive analysis and experimental demonstrations have established the temporal advantages of event-driven sensors over conventional frame-based imagers [11]. Nonetheless, comparing the two architectures under I/O-constrained conditions with all other variables held constant remains instructive.

Maximum Effective Frame Rate

In conventional frame-based imagers, pixels are read out sequentially under the control of a synchronous frame timer. In practice, the achievable frame rate is limited by several factors, including pixel integration time, pixel-to-column charge transfer time, analog-to-digital conversion time, and I/O bandwidth. Advances in visible CMOS image sensors and readout integrated circuits (ROICs) have enabled pipelining of these operations, such that the maximum frame rate can be ultimately constrained by the I/O bandwidth [12]. Achieving ultra-high frame rates in large-format imagers with column-parallel A/D conversion therefore requires a large number of high-speed I/O channels operating near their maximum data rates [13].

In contrast, event-driven sensors report pixel activity only when a sufficient change in intensity is detected over time. That is, event-driven cameras respond to variations in temporal contrast within the scene. Pixel events are processed in a time-ordered manner, with each event encoding the pixel location (x,y) and the direction of the intensity change (polarity). These events are transmitted off-chip in the order in which they are generated, forming an address-event representation (AER) data stream [6, 7]. Optional time-stamping can be applied by on- or off-chip processing units to record the arrival time of each event, although this is not considered in the present analysis.

Fig. 1 illustrates conceptual timing diagrams for both event-based and frame-based cameras. High-speed I/O interfaces typically allocate a portion of the available bandwidth to protocol overhead, including headers and footers that define packet boundaries and support clock and data recovery. This overhead (η_{ovrhd}) is represented by the pale yellow packets in Fig. 1.

In the frame-based camera timing (top), valid line data consists of a continuous stream of digitized pixel values across all columns in a given row. These values are typically generated by an analog-to-digital converter (ADC), with the bit depth determined by the converter resolution. Transmission of a full frame requires all rows to be read out sequentially. This can be accomplished using a single I/O port, transmitting one line at a time, or multiple parallel I/O ports, denoted by k_p in Fig. 1. Increasing the I/O data rate ($f_{I/O}$), reducing ADC bit depth (N_{adc}), or increasing the number of parallel ports all serve to increase the I/O-limited frame rate for a given array format in conventional image sensors, as described by (1).

$$\text{Frame Rate [fps]} = \frac{(1-\eta_{ovrhd})k_p f_{I/O}}{N_{pix}N_{adc}} \tag{1}$$

In the event-based camera timing (bottom), pixel data are not read out sequentially. Instead, events are generated asynchronously and transmitted off-chip in a time-ordered, first-come, first-served manner. Each event is encoded in AER format, consisting of the pixel coordinates (x,y) and a polarity bit, where "1" denotes an ON event and "0" denotes an OFF event. Because each event carries its own spatial address, the number of bits per event increases with array size. Since frames represent fully sampled spatial snapshots of the pixel array at a given time, it is not meaningful to define a true frame rate for an event-based sensor. Instead, an effective frame rate is defined to quantify the maximum rate at which sparse scene information (η_{scene}) can be transmitted off-chip, as given in (2).

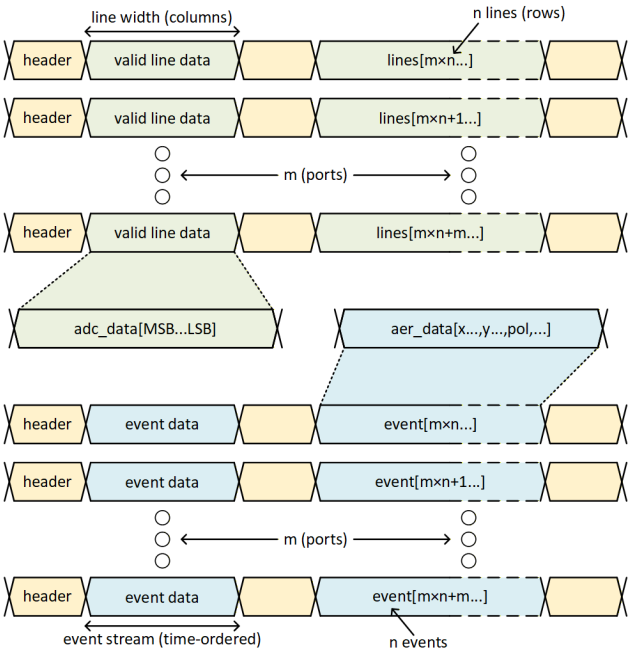

Figure 1. *Conceptual I/O timing diagram for frame-based (top, green) and event-based (bottom, blue) image sensors.*

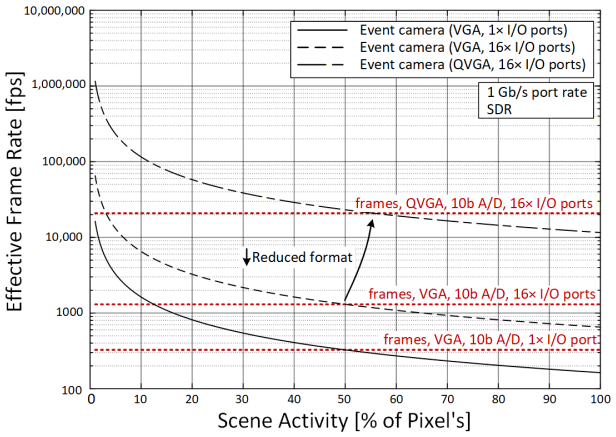

Figure 2. *Maximum effective frame rate versus spatial scene activity for I/O limited event (black) and frame (red) cameras.*

$$\text{Eff. Frame Rate [fps]} = \frac{(1-\eta_{ovrhd})k_p f_{I/O}}{\eta_{scene} N_{pix}(\log_2 m + \log_2 n + 1)} \quad (2)$$

The effective frame rate increases with decreasing array size and reduced scene activity. This behavior is illustrated in Fig. 2, where the maximum achievable effective frame rate is compared between event-based and frame-based cameras for different array formats across a varying level of pixel activity.

As shown in Fig. 2, reducing scene activity provides event-driven cameras with significantly greater headroom to increase effective frame rate compared to frame-based cameras, which must read out all pixels regardless of activity. In both modalities, increasing the number of I/O ports or reducing array size leads to higher effective frame rates. However, for each configuration, there exists a level of scene activity, or spatial density of pixels undergoing temporal change, at which the event-based and frame-based sensors achieve equivalent effective frame rates. This crossover arises because each event encodes both spatial address and polarity, resulting in 18-bit and 20-bit per-pixel transmissions for QVGA and VGA formats, respectively. This exceeds the per-pixel data payload of frame-based readout with a 10-bit column-parallel ADC. Consequently, as scene sparsity decreases, the advantage of event-driven sensors in maximizing effective frame rate diminishes.

Latency vs. Bitrate

Conventional image sensors address latency by increasing the frame rate, thereby sampling the scene more frequently [14]. However, this approach leads to a substantial increase in bit rate, particularly for large-format imagers. I/O interfaces in image sensor-compatible process technologies are limited in speed, and even with techniques such as double data rate (DDR), I/O bandwidth remains a fundamental constraint. In contrast, event-driven sensors are not required to read out every pixel. Instead, only pixels undergoing temporal change are transmitted, and the resulting latency is fundamentally determined by the pixel response time, typically on the order of microseconds [3, 4, 5].

This concept is highlighted in Fig. 3, which depicts the classical trade-off between bitrate and latency in frame-based imagers, with event-driven camera performance overlaid for varying levels of scene activity and relative pixel power consumption.

Fig. 3 illustrates an I/O-limited QVGA array with a varying number of I/O ports operating at a fixed data rate of 2 Gb/s per port. In frame-based imagers, latency and frame rate are inherently coupled, such that achieving microsecond-scale latency requires frame rates on the order of hundreds of kiloframes per second and aggregate bit rates in the hundreds of gigabits per second.

In contrast, event-driven sensors in the visible regime have demonstrated photocurrent-to-event latencies on the order of 10 μs [3, 4, 5], corresponding to effective frame rates exceeding 50 kfps. In this case, the bit rate is governed by the level of scene activity, increasing as more pixels generate events within a given temporal window.

As shown in Fig. 3, event-driven sensors ultimately approach the same I/O bandwidth limit as frame-based sensors. This occurs at approximately 50% scene activity for the configurations considered, consistent with the trends observed in Fig. 2, and arises from the higher per-pixel data payload associated with event encoding. In sparse scenes, event-driven cameras achieve low-latency at orders-of-magnitude lower bit rates. However, as scene sparsity decreases, they become increasingly constrained by the same I/O bottleneck that limits conventional frame-based imagers.

Pixel power can be traded directly against event latency, with the resulting impact on throughput demonstrated in Fig. 3. The blue shaded region denotes data rates achievable using a single I/O port under the given constraints. Event-driven sensors operating within this regime can therefore achieve extremely low-latency at a fraction of the single-port I/O power, particularly in sparse scenes. Conversely, improving event latency requires increased pixel power to enhance the gain–bandwidth performance of the TIA front-end.

Event-Driven Sensors for Infrared Imaging

Two unit-cell front-ends are considered in this section operating with both LOG and LIN mode TIAs. A micrograph of a demonstration ROIC with coincident 32×32 test arrays is shown in Fig. 4 (top). The results presented in this section for CS and MET versus ambient background are derived from experimental measurements obtained from preliminary ROIC characterization. The experimental results quantify the input-referred noise of the sensor across a wide range of ambient current levels at the TIA input. These measurements are utilized in the results and discussion presented in this section and throughout the remainder of the manuscript.

The unit cell of an event-driven pixel contains significantly more circuitry than that of a conventional frame-based pixel, requiring approximately 12–15 additional transistors [11]. An abridged schematic of a representative event-based pixel, with key functional regions highlighted, is shown in Fig. 4 (bottom). This increased complexity arises from the inclusion of a continuous-time transimpedance amplifier (TIA) to convert photocurrent into voltage, along with an AC-coupled, self-resetting change detector (CD). The CD differentiates and thresholds the TIA output, enabling the pixel to respond only to changes that exceed a predefined photocurrent threshold.

Given the limitations of conventional TIA front-ends under long-wavelength (λ_c) IR photodiode operating conditions, alternative architectures with improved robustness are warranted for event-driven IR imaging.

The Dark and Background Current Problem

A primary challenge in achieving feasible event-driven IR sensing at long cutoff wavelengths (e.g., MWIR and LWIR) lies in the pixel front-end. In emissive bands employing photodiodes with cutoff wavelengths greater than 4 μm, both dark current and background photocurrent can be substantial and often exceed the signal photocurrent associated with the target thermal signature. This is illustrated in Fig. 4, where arrows indicate the relative magnitudes of these current components.

Conventional event-driven pixels typically employ a LOG TIA, in which the feedback element (Z_{fb}) produces an output voltage proportional to the natural logarithm of the total input current. While this architecture provides high transimpedance gain and strong sensitivity at low signal and background currents (I_0,

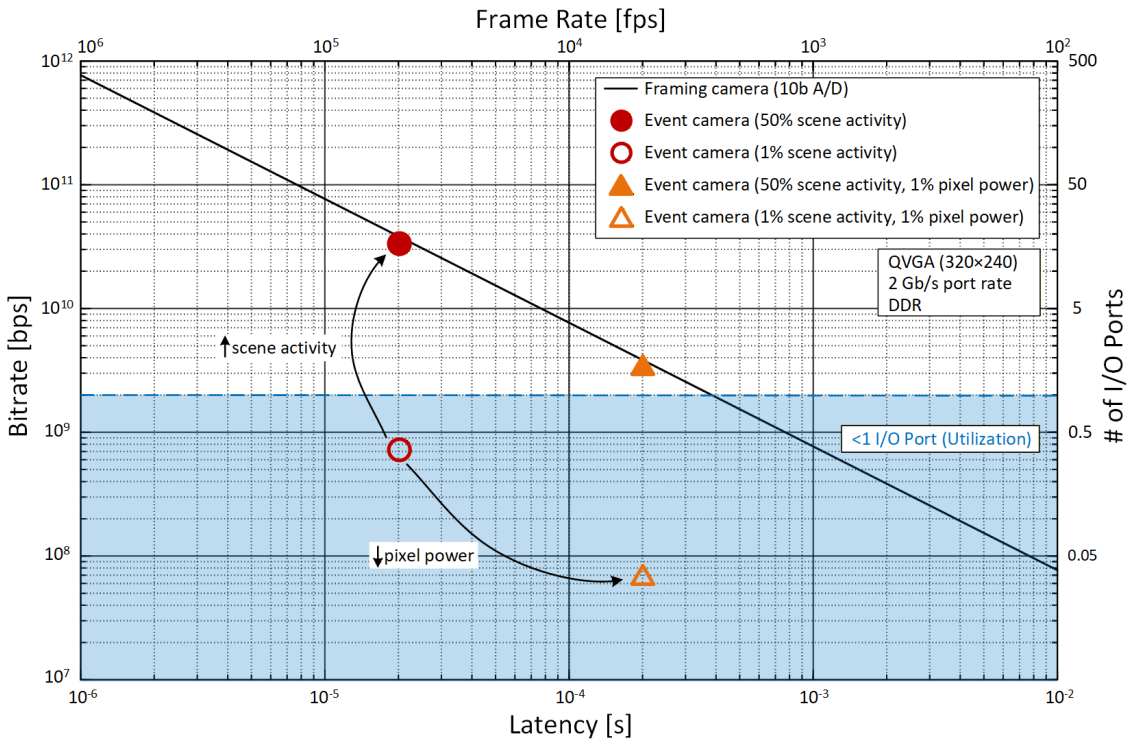

Figure 3. *Bitrate versus latency for frame (black, solid line) and event (circles, triangles) cameras.*

i_{bkg}), its inherently compressive response becomes detrimental at longer cutoff wavelengths (λ_c) and under high operating temperature (HOT) conditions. The transimpedance gain and the resulting change in photoreceptor voltage (ΔV_p) for background limited conditions (BLIP) is given by (3).

$$\Delta V_{p,LOG} = \Delta i_{ph} Z_{fb}(i_{ph}, I_0, i_{bkg}) \approx \eta V_T \ln\left(\frac{i_{bkg} + \Delta i_{ph}}{i_{bkg}}\right) \tag{3}$$

Here, η denotes the transistor ideality factor and V_T the thermal voltage. In practice, a transistor biased in subthreshold is typically used to implement Z_{fb} and achieve the logarithmic response at the pixel output [3, 5]. Alternative front-end architectures without a TIA have also been proposed in the literature [15].

Even under BLIP conditions, the background photocurrent i_{bkg} can be sufficiently large to significantly attenuate the TIA response and degrade the achievable contrast in event-driven IR pixels. Fig. 5 illustrates the response of a conventional LOG front-end pixel under increasing background flux, shown in terms of both ambient scene temperature and the corresponding photodiode current density for the parameters specified in the figure. Superimposed curves indicate the required contrast sensitivity (CS), defined as the ratio of detectable photocurrent to i_{bkg} and expressed as a percentage, for detecting a thermal change of 500 mK. The system-level parameters of a 5 μm cutoff wavelength (λ_c), 50% quantum efficiency, and $f/2$ optics are representative of modern MWIR imaging systems [10].

Two contrast sensitivity (CS) cases are shown: one for a target fixed at 300 K and one for a target at the ambient background temperature, indicated by the solid black and dashed red curves, respectively. In both cases, the CS requirement becomes more stringent at higher background levels, as the background flux increases more rapidly than the differential flux produced by a 500 mK thermal contrast. As a result, the required CS approaches and falls below 2% for ambient backgrounds near and above room temperature (300 K). Achieving CS on the order of 2% is demonstrated by state of the art visible event-based sensors in research settings and remains a challenging benchmark across spectral bands [16, 17].

In addition to the stringent CS requirements imposed on IR sensors operating at sub-kelvin thermal differentials, the relative contrast (C) also degrades with increasing background. As previously discussed, this degradation arises from the influence of i_{bkg} and I_0 on the TIA transimpedance gain, exemplified in Fig. 4. Even when neglecting the contribution of I_0 and assuming high quality detector material with minimal defects, which is challenging to achieve at long λ_c [10], the degradation in C over a 100 K increase in ambient background temperature exceeds 40% under the conditions specified in the figure.

For event generation at low thermal differentials using traditional LOG front-ends, increasingly low CS is required under background conditions that simultaneously degrade the achievable contrast. This combination imposes stringent and often competing requirements on the pixel front-end to achieve both high dynamic range and sensitivity. Given the sensitivity of traditional TIA front-ends to the characteristics of long-cutoff-wavelength IR photodiodes, it is important to explore alternative front-end architectures that are more robust to the operating conditions of

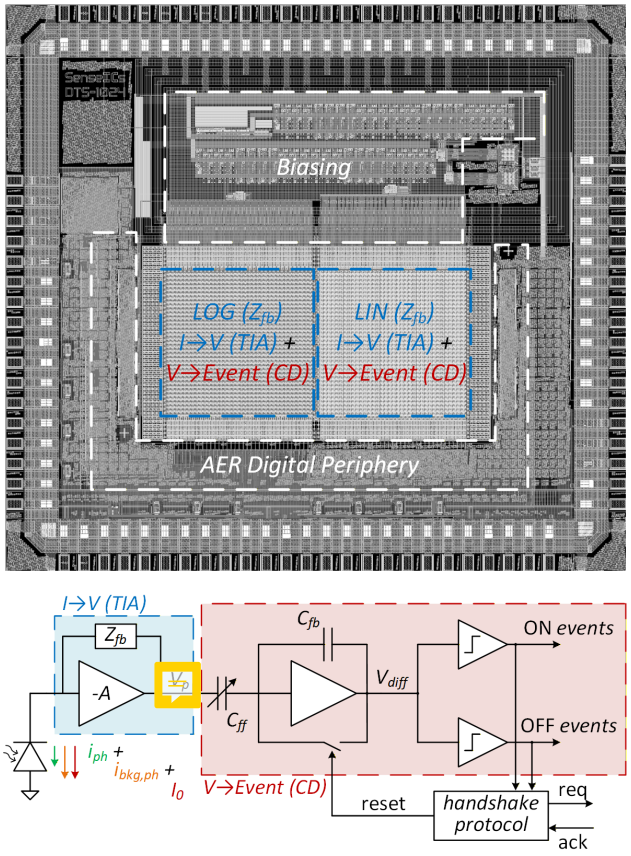

Figure 4. *Die micrograph of the demonstration chip fabricated with both logarithmic (LOG) and linear (LIN) front-ends. Abridged schematic of a conventional event-driven pixel. Arrows adjacent to the photodiode indicate the relative magnitudes of dark current (I_0), background photocurrent (i_{bkg}), and signal photocurrent (i_{ph}).*

event-driven IR imaging.

Relative Performance of Logarithmic (LOG) vs. Linear (LIN) Front-Ends

The principal source of performance degradation in event-driven IR pixels is the compressive response of LOG front-ends under high I_0 and i_{bkg}. While this response enables ultra high transimpedance gain when paired with silicon photodiodes, it compresses significantly under the elevated dark current of III–V photodiodes and the high background flux present in thermally emissive spectral bands. This strongly motivates the use of a linear front-end, in which the transimpedance gain remains invariant with input current, ensuring stable gain across a wide range of background flux and dark current conditions.

A front-end TIA with linear response is straightforward to describe. In practice, however, photocurrents of interest remain small even in the IR spectrum, making a purely linear feedback element insufficient to provide adequate conversion gain. Consequently, a generalized linear current gain (G_{LIN}) is considered in this analysis. By substituting a linear feedback element into the TIA shown in Fig. 4 (bottom), the front-end gain can be expressed

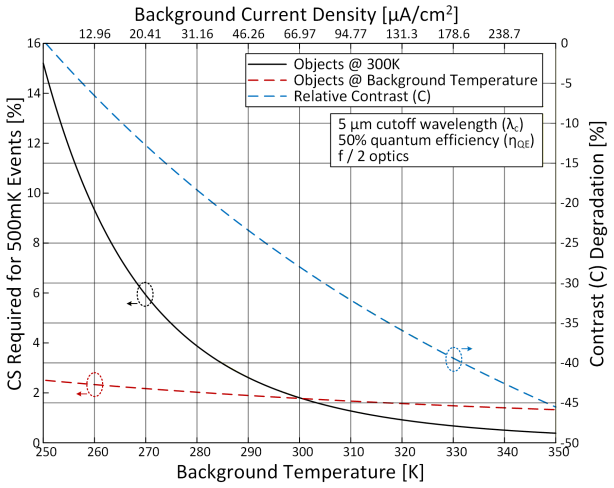

Figure 5. *Contrast sensitivity (CS) required for event generation at a 500 mK thermal differential, and event-driven contrast (C) degradation as a function of ambient background.*

as in (4).

$$\Delta V_{p,LIN} = \Delta i_{ph} G_{LIN} Z_{fb} = \Delta i_{ph} A_{CG} \tag{4}$$

In this formulation, G_{LIN} and Z_{fb} are independent of i_{ph}, I_0, and i_{bkg}, in contrast to (3). As a result, the front-end transfer function in the LIN case is non-compressive, leading to a reduction in dynamic range that can be traded for A_{CG}. This enables contrast sensitivity (CS) to decrease linearly with increasing background, since the sensitivity is invariant with respect to i_{bkg}. Contrast sensitivity for both LOG and LIN pixel front-ends are shown below in (5) and (6), respectively.

$$CS_{LOG} \approx \frac{\Delta i_{ph,ev}}{i_{bkg}} = \exp\left(\frac{\theta_{th}}{\frac{C_{ff}}{C_{fb}} \eta V_T}\right) - 1 \tag{5}$$

$$CS_{LIN} \approx \frac{\Delta i_{ph,ev}}{i_{bkg}} = \left(\frac{\theta_{th}}{i_{bkg} \frac{C_{ff}}{C_{fb}} G_{LIN} Z_{fb}}\right) \tag{6}$$

Where $\Delta i_{ph,ev}$ denotes the minimum detectable photocurrent and θ_{th} is the programmable event threshold, assumed to be identical for ON and OFF events in this analysis. For the LOG case (CS_{LOG}), the transimpedance gain is inversely proportional to i_{bkg}, resulting in contrast sensitivity that is first-order invariant with respect to i_{bkg}. As i_{bkg} increases, $\Delta i_{ph,ev}$ increases proportionally, leading to degraded absolute sensitivity ($\Delta i_{ph,ev}$) under high background conditions. In the LIN case (CS_{LIN}), the transimpedance gain is independent of i_{bkg} to the first order, resulting in improved contrast sensitivity with increasing i_{bkg}, as $\Delta i_{ph,ev}$ remains constant.

Reduced CS at higher background corresponds to improved sensitivity and a lower minimum event temperature (MET), which defines the minimum resolvable temperature change required to

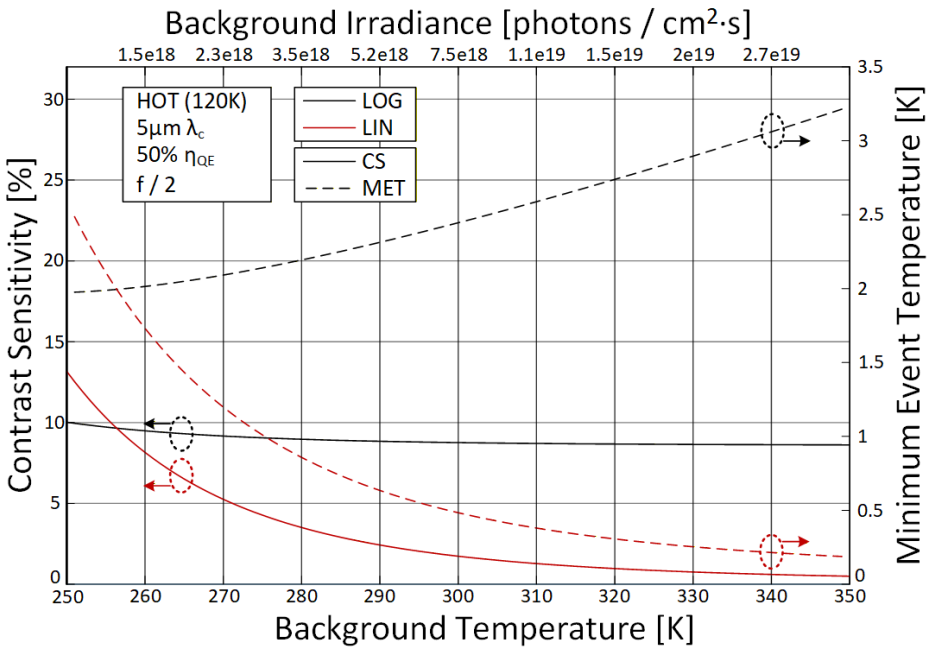

Figure 6. *Contrast sensitivity (solid) and minimum event temperature (dashed) as functions of ambient background for logarithmic (LOG, black) and linear (LIN, red) pixel front-ends.*

trigger an event. MET expressions for both LOG and LIN pixel front-ends are shown below in (7) and (8), respectively.

$$MET_{LOG} \approx \frac{\Delta i_{ph,ev}}{\Delta i_{ph,1K}} = \left(\frac{i_{bkg}}{\Delta i_{ph,1K}}\right)\left[\exp\left(\frac{\theta_{th}}{\frac{C_{ff}}{C_{fb}}\eta V_T}\right) - 1\right] \tag{7}$$

$$MET_{LIN} \approx \frac{\Delta i_{ph,ev}}{\Delta i_{ph,1K}} = \left(\frac{1}{\Delta i_{ph,1K}}\right)\left(\frac{\theta_{th}}{\frac{C_{ff}}{C_{fb}} G_{LIN} Z_{fb}}\right) \tag{8}$$

Where $\Delta i_{ph,1K}$ is the photocurrent normalized to a 1 K scene temperature differential at a given background condition. For both expressions, MET is directly proportional to CS, which is nearly constant with background (neglecting noise impacts) for the LOG front-end. The expressions differ most significantly because MET_{LOG} is directly proportional to i_{bkg}, while MET_{LIN} is invariant.

The above sensitivity analysis is illustrated in Fig. 6, which shows CS and MET as functions of background for both LOG and LIN front-end architectures. The results presented in this figure are derived from a combination of first-principles photodetector modeling, pixel circuit simulations, and experimental measurements of input-referred noise obtained using the demonstration ROIC shown in Fig. 4.

For the LOG front-end, the transimpedance gain is strongly dependent on the magnitude of the i_{bkg} and largely governs the system dynamics. CS_{LOG} remains approximately constant, as shown in (5), as a function of background. It increases slightly at low background levels, where transimpedance gain rises, input-referred TIA noise is minimized, and shot noise becomes non-negligible. However, MET_{LOG} increases with background despite the nearly constant CS_{LOG}, due to the reduction in transimpedance gain and the associated loss in sensitivity. This is evident in (7), where the increase is driven by i_{bkg} rising faster than the normalized differential photocurrent ($\Delta i_{ph,1K}$) under the optical system assumptions used in the plot sub-panel.

In contrast, the LIN front-end exhibits improved CS_{LIN} and MET_{LIN} performance at higher background levels, owing to its conversion gain being independent of i_{bkg}, as shown in (6). As the ambient background increases, the conversion gain remains constant while $\Delta i_{ph,1K}$ increases, enhancing sensitivity to temperature changes. Not shown in Fig. 6 is the saturation point of the LIN front-end, which occurs earlier than for the LOG front-end and depends on the linear gain G_{LIN}.

Both architectures exhibit degraded CS at low background levels, where smaller $\Delta i_{ph,1K}$ results from a given temperature variation, requiring larger temperature differences to trigger events. This behavior is consistent with the classical dependence of noise equivalent temperature difference (NETD) on scene flux [18]. From this analysis, two key observations emerge: (1) LIN front-end operation is robust to high background flux to the first order, and (2) LOG front-end operation is advantageous at low background, consistent with its effectiveness in low-I_0 and low-i_{bkg} visible event-driven imagers.

Conclusion

This work highlights the system-level and pixel-level trade-offs in event-driven infrared imaging. Under I/O-limited conditions, event-driven sensors achieve superior effective frame rate and latency in sparse scenes, with diminishing advantage as scene activity increases. At the pixel level, conventional LOG front-ends degrade under elevated dark current and background

flux, limiting contrast sensitivity and minimum event temperature. Comparative analysis shows that LIN front-ends maintain stable conversion gain and improved sensitivity at high background, while LOG architectures remain advantageous at low background. These results define operating regimes for both event-driven and frame-based imaging approaches and guide front-end selection for infrared event-driven sensors.

References

[1] C. Mead and M. Mahowald, The silicon retina, Sci. Amer., 1994.

[2] T. Delbruck and C. Mead, Adaptive photoreceptor with wide dynamic range, Proc. IEEE ISCAS, vol. 4, pp. 339–342 (1994).

[3] P. Lichtsteiner, C. Posch, and T. Delbruck, A 128x128 120 dB 15 us latency asynchronous temporal contrast vision sensor, IEEE J. Solid-State Circuits, 2008.

[4] M. Guo et al., A three-wafer-stacked hybrid 15-MPixel CIS + 1-MPixel EVS with 4.6-GEvent/s readout, IEEE J. Solid-State Circuits, 58, 2955–2964 (2023).

[5] C. Posch, A QVGA 143 dB dynamic range frame-free PWM image sensor, IEEE J. Solid-State Circuits, 2011.

[6] K. A. Boahen, A burst-mode word-serial address-event link I: transmitter design, IEEE Trans. Circuits Syst. I, 51, 1269–1280 (2004).

[7] K. A. Boahen, A burst-mode word-serial address-event link II: receiver design, IEEE Trans. Circuits Syst. I, 51, 1281–1291 (2004).

[8] Prophesee, Event-Based Vision Applications, Available: https://www.prophesee.ai/event-based-vision-applications/

[9] DARPA, Fast Event-based Neuromorphic Camera and Electronics (FENCE), 2024.

[10] A. Rogalski et al., Trends in performance limits of HOT infrared photodetectors, Appl. Sci., 11 (2021).

[11] G. Gallego et al., Event-based vision: A survey, IEEE Trans. Pattern Anal. Mach. Intell., 44, 154–180 (2022).

[12] S. Huang et al., Design of analog readout circuitry with front-end multiplexing, Proc. IISW, 2013.

[13] A. Agarwal et al., A 316MP 120FPS high dynamic range CMOS image sensor, Sensors, 23 (2023).

[14] A. Agarwal et al., High-frame-rate low-noise global shutter CMOS image sensor, Sensors, 26 (2026).

[15] P. Fernández-Peramo et al., A photovoltaic dynamic vision sensor, IEEE J. Solid-State Circuits, 2025.

[16] T. Serrano-Gotarredona and B. Linares-Barranco, A 128x128 asynchronous dynamic vision sensor with 1.5% contrast sensitivity, IEEE J. Solid-State Circuits, 2013.

[17] M. Yang, S.-C. Liu, and T. Delbruck, A dynamic vision sensor with 1% contrast sensitivity, IEEE J. Solid-State Circuits, 2015.

[18] E. L. Dereniak and G. D. Boreman, Infrared Detectors and Systems, Wiley-Interscience, 1996.

Author Biography

Dr. Roman Fragasse is a Senior Design Engineer at SenseICs Corporation. He earned his B.S., M.S., and Ph.D. degrees in Electrical and Computer Engineering from The Ohio State University in 2016, 2018, and 2025, respectively. His current work focuses on mixed-signal design for high-performance CMOS image sensors and readout integrated circuits (ROICs) for passive EO/IR imagers, LiDAR receivers, and event-driven image sensors. Roman has authored or co-authored 13 journal and conference publications.

JOIN US AT THE NEXT EI!

electronic IMAGING

Imaging across applications . . . Where industry and academia meet!

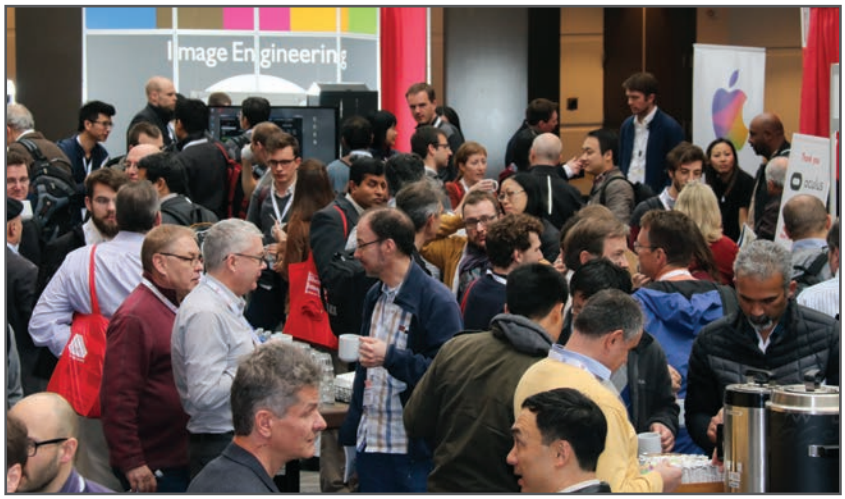

• SHORT COURSES • EXHIBITS • DEMONSTRATION SESSION • PLENARY TALKS •
• INTERACTIVE PAPER SESSION • SPECIAL EVENTS • TECHNICAL SESSIONS •

www.electronicimaging.org

ADVANCING IMAGING SCIENCE 75 1947 IS&T 2022 imaging.org